Supporting Information

Superimposed OER and UOR performances by the interaction of each component in Fe–Mn electrocatalyst

Xin-ying Meng [a,b,#], Meng Wang [a,b,#], Yicong Zhang [b], Zhihao Li [b], Xiaogang Ding [b], Weiquan Zhang [b], Can Li [a, b] and Zhen Li [a,b,*]

a. Shenzhen Research Institute of Northwestern Polytechnical University, Shenzhen, 518000, P. R. China.

b. State Key Laboratory of Solidification Processing, Center for Nano Energy Materials, School of Materials Science and Engineering, Northwestern Polytechnical University and Shaanxi Joint Laboratory of Graphene (NPU), Xi'an, 710072, P. R. China.

E-mail: lizhen@nwpu.edu.cn

[#] These authors contribute equally

Experimental Section

Materials: Manganese acetate tetrahydrate ($MnC_4H_6O_4 \cdot 4H_2O$), ferrous sulfate ($FeSO_4 \cdot 7H_2O$) and sodium hypophosphite monohydrate ($NaH_2PO_2 \cdot H_2O$) were purchased from Macklin Biochemical Co., Ltd (Shanghai, China). Ammonium chloride (NH_4Cl) and Nafion solution (5%) were purchased from Aladdin Industrial Corporation (Shanghai, China). Potassium hydroxide (KOH) and urea were purchased from Guangdong Guanghua Sci-Tech Co., Ltd. The nickel foam (NF) was obtained from Kunshan Guangjiayuan new materials Co. Ltd. All reagents were used as received. The NF (1×2 cm^2) was washed ultrasonically in 1 M HCl, ethanol and deionized water for 10 min sequentially, and dried at 60 °C for 4 h.

Synthesis of FeMn-PS compositions: All electrochemical deposition was carried out using a CHI 760D electrochemistry workstation (CHI Instrument, China) with a three-electrode setup. $FeMn_x$-PS was synthesized by in situ electrodeposition method. The cleaned Ni foam (NF, 1×2 cm^2) was used as the working electrode; a Pt plate and saturated Ag/AgCl electrode were used as the counter and reference electrode, respectively. The electrolyte was attained by dissolving 0.2 mol $MnC_4H_6O_4 \cdot 4H_2O$, 0.2 mol $FeSO_4 \cdot 7H_2O$, 1 mol NH_4Cl and 1 mol $NaH_2PO_2 \cdot H_2O$ in 50 mL H_2O. Before electrodeposition, the electrolyte was saturated with Ar for 30 min to remove O_2. The electrodeposition process

was carried out at 2.5 mA·cm^{-2} for 60 s. Then, the NF was washed with water, and dried at 60°C overnight. The obtained samples were denoted as FeMn-PS. Fe-PS, Mn-PS, FeMn$_{0.2}$-PS, FeMn$_{0.6}$-PS and FeMn$_{1.4}$-PS were prepared in the same way, except that the mole ratio of Mn/Fe in the precursor changes to 0:1, 1:0, 0.2:1, 0.6:1 and 1.4:1. The total amount of metal (Fe+Mn) was kept at 0.4 mol in the precursors. In addition, we prepared FeMn-S without adding NaH$_2$PO$_2$·H$_2$O in the precursor, and FeMn-P with FeCl$_2$ instead of FeSO$_4$·7H$_2$O in the precursor.

Characterization: The crystalline structure of the as-obtained catalyst was characterized by X-ray diffraction pattern (XRD, D8 Advance powder X-ray diffractometer, Cu Kα radiation, λ=0.15418 nm). Scanning electron microscopy (SEM, ZEISS Sigma 300) and transmission electron microscopy (TEM, FEI Talos F200X) were employed to characterize the morphology and microstructure of the catalyst. The Raman spectrum was recorded on a Renishaw in Via Raman microscope with a 532 nm laser. Fourier transform infrared spectroscopy (ATR-FTIR) data were collected on Bruker in TENSOR II. The elemental composition and electronic state of the catalyst were analyzed by X-ray photoelectron spectroscopy (XPS, AXIS ULTRA spectrometer).

Electrochemical measurements: All electrochemical measurements were carried out on a CHI 760D electrochemistry workstation (CHI Instrument, China) by a three-electrode system. The catalyst-loaded NF (1

× 1 cm^2), a Pt plate and saturated Ag/AgCl electrode were used as the working electrode, reference electrode and counter electrode，respectively. The electrolytes for OER and UOR tests were 1 M KOH and 1 M KOH with 0.33 M urea, respectively. All potentials measured vs. Ag/AgCl were converted to the reversible hydrogen electrode (RHE) as: E (RHE) = E (Ag/AgCl) + 0.197 V + 0.059 pH. Linear sweep voltammetry (LSV) curves were recorded with a scan rate of 5 mV s^{-1} (with iR compensation) to evaluate the overpotential of OER and UOR. Electrochemically active surface area (ESCA) was studied by measuring the electrochemical double-layer capacitance (C_{dl}) from cyclic voltammetry (CV) curves at different scan rates. Electrochemical impedance spectroscopy (EIS) measurements were recorded at 1.5 V vs. RHE over a frequency range of 10^5 to 10^{-2} Hz.
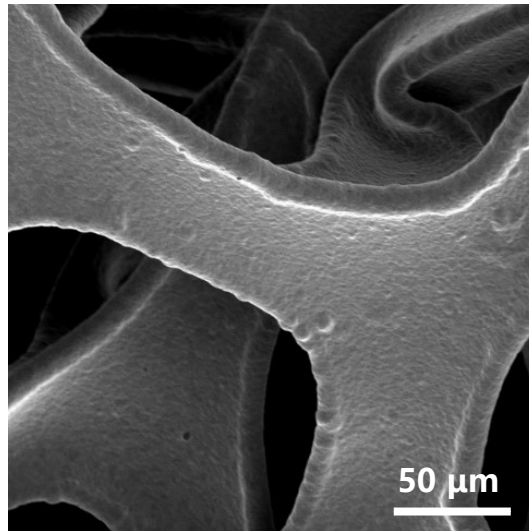
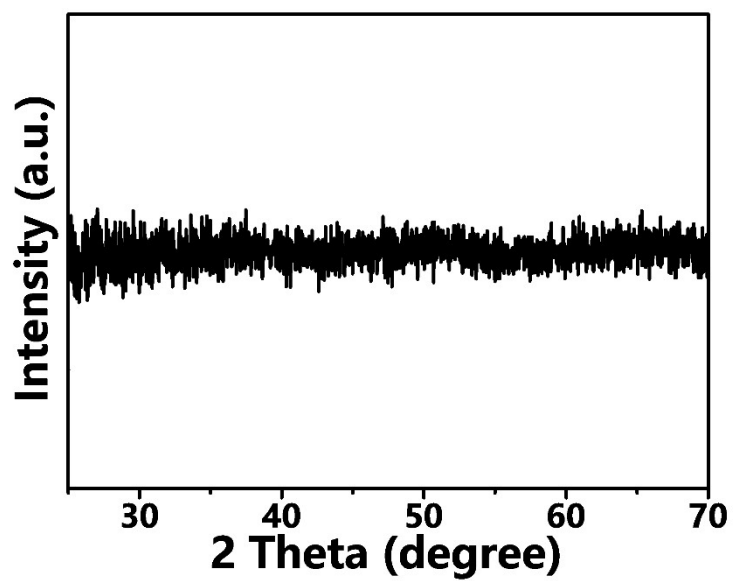**Fig. S1.** SEM image of pure NF substrate.

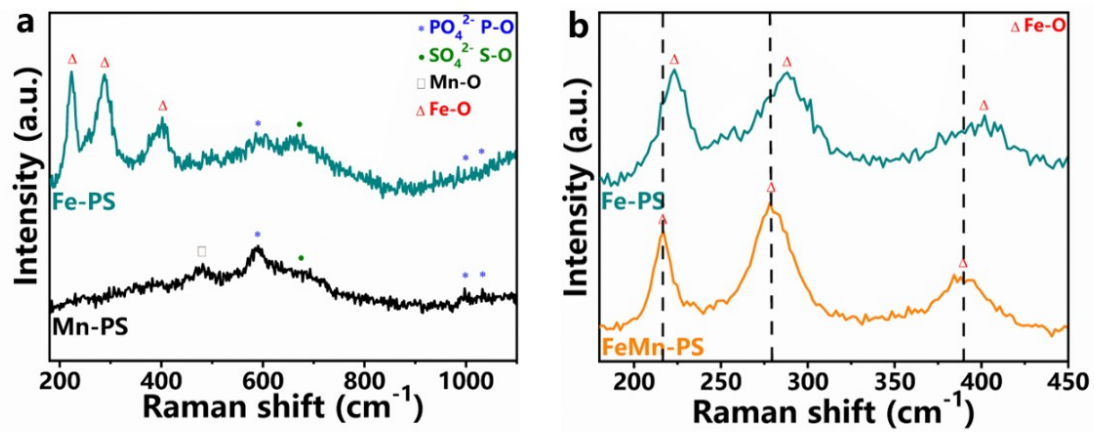**Fig. S2.** XRD pattern of the FeMn-PS catalyst.

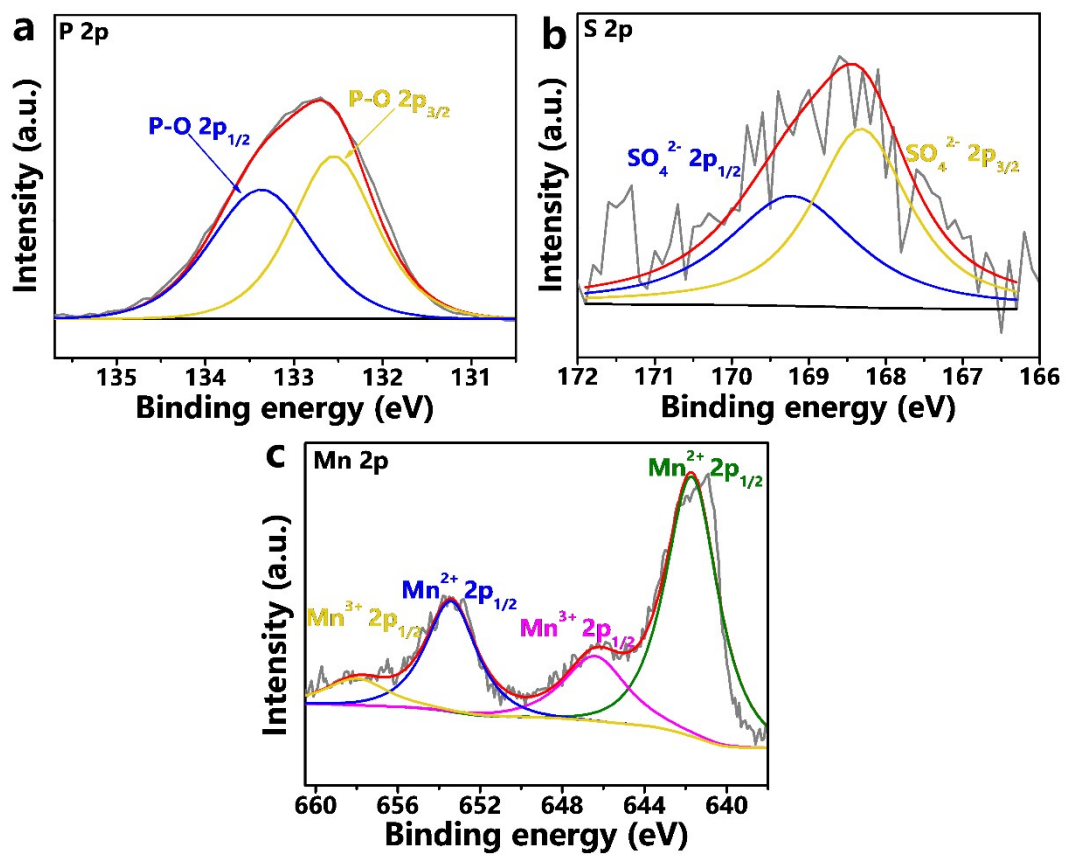**Fig. S3.** (a) Raman spectra of Fe-PS and Mn-PS. (b) Raman spectra of Fe-PS and FeMn-PS.

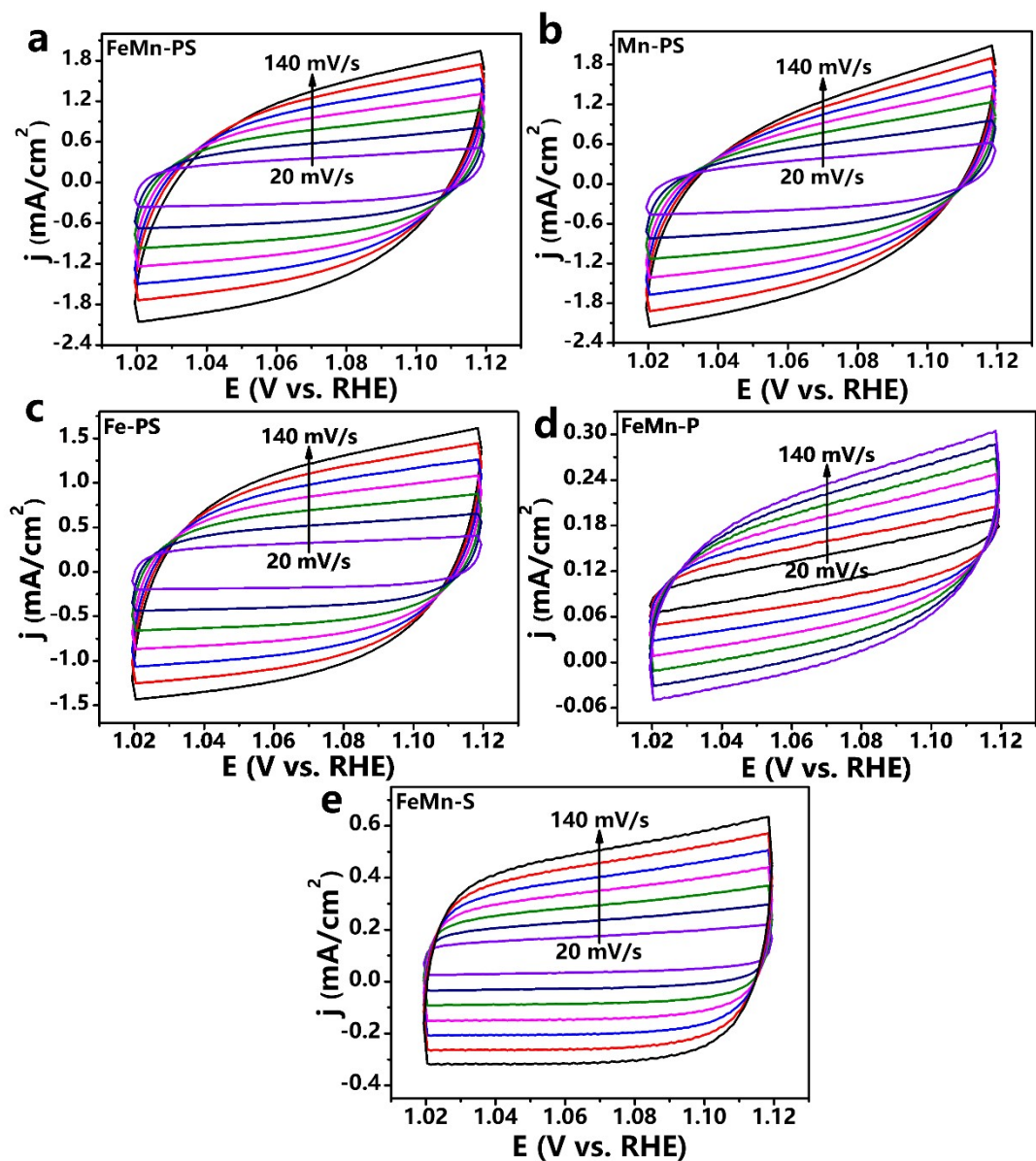**Fig. S4.** High resolution XPS spectra for (a) P 2p, (b) S 2p and (c) Mn 2p of FeMn-PS.

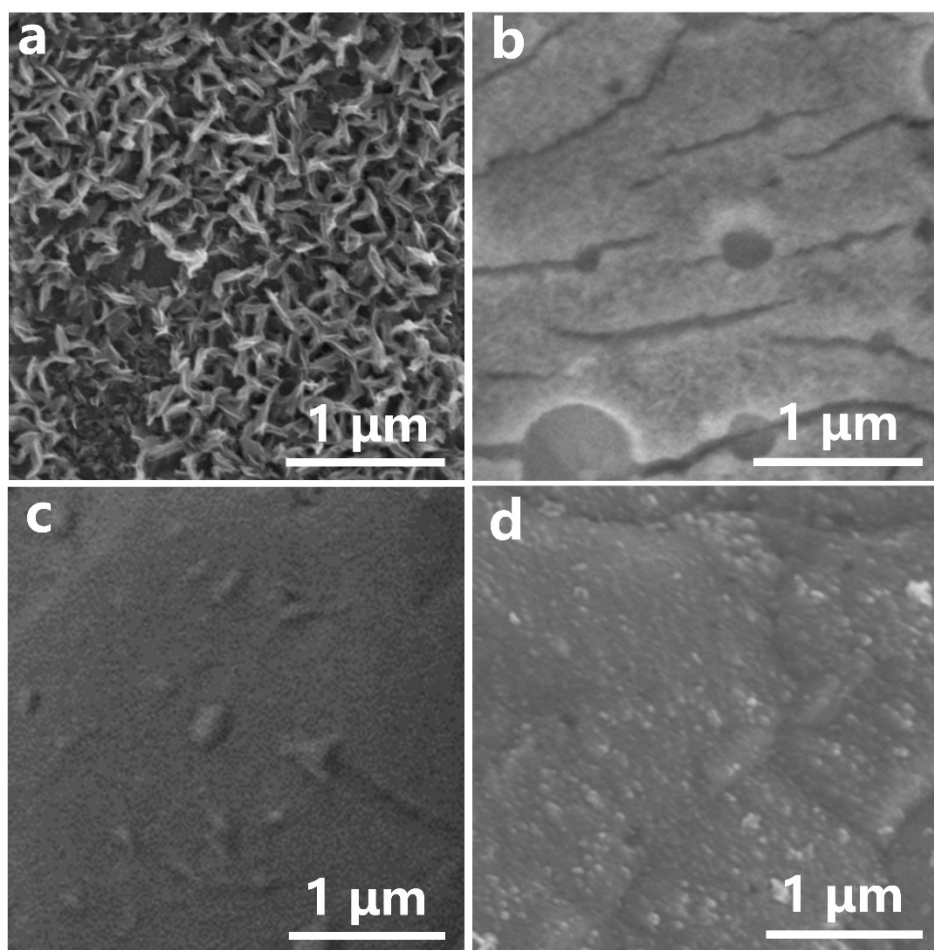**Fig. S5.** CV curves at different scan rates for: (a) FeMn-PS, (b) Mn-PS, (c) Fe-PS, (d) FeMn-P and (e) FeMn-S.

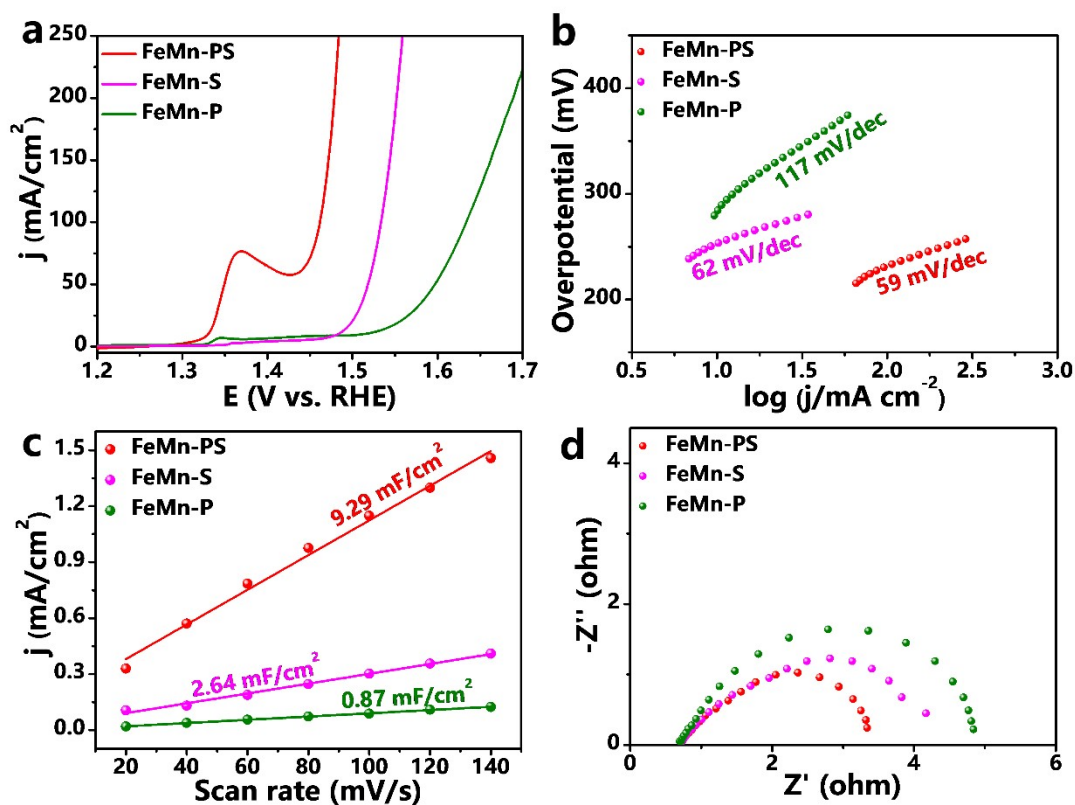**Fig. S6.** SEM image of (a) Fe-PS, (b) Mn-PS, (c) FeMn-P, (d) FeMn-S.

Fig. S7. OER performance. (a) Polarization curves of FeMn-PS, FeMn-S and FeMn-P in O_2-saturated 1 M KOH electrolyte. (b) Tafel plots of FeMn-PS, FeMn-S and FeMn-P. (c) Nyquist plots of FeMn-PS, FeMn-S and FeMn-P at an overpotential of 270 mV. (d) Plots of current density at 1.07 V vs different scan rates for FeMn-PS, FeMn-S and FeMn-P.
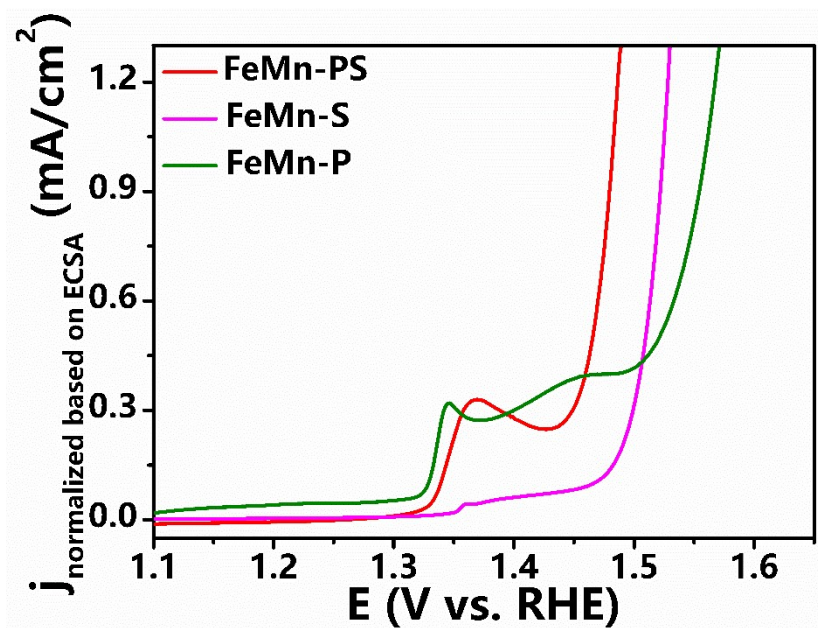
Fig. S8. ECSA normalized LSV curves of FeMn-PS, FeMn-S and FeMn-P in O₂-saturated 1 M KOH electrolyte.
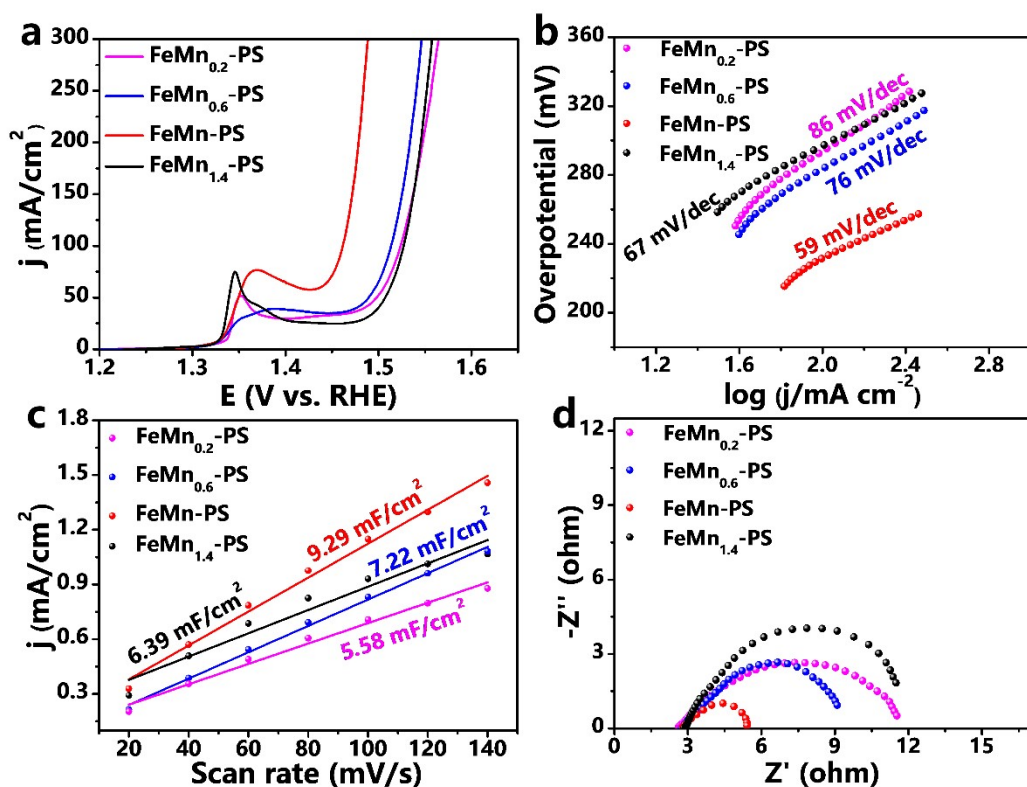
Fig. S9. (a) OER polarization curves, (b) corresponding Tafel plots, (c) Electrochemically active surface area (ECSA) and (d) Nyquist plots of pristine FeMn$_{0.2}$-PS, FeMn$_{0.6}$-PS, FeMn-PS, FeMn$_{1.4}$-PS for OER test.
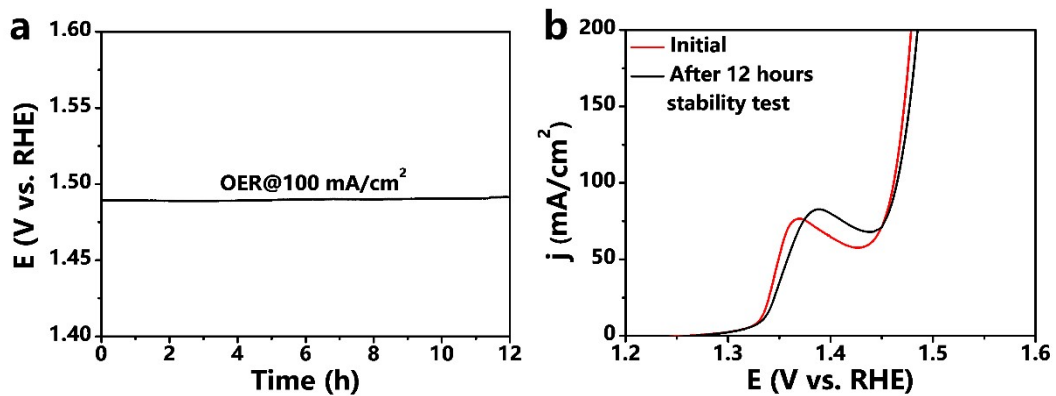
Fig. S10. (a) Chronopotentiometric curves of FeMn-PS in 1 M KOH electrolyte. (b) LSV curves of the FeMn-PS initial and after 12 hours stability test in 1 M KOH.
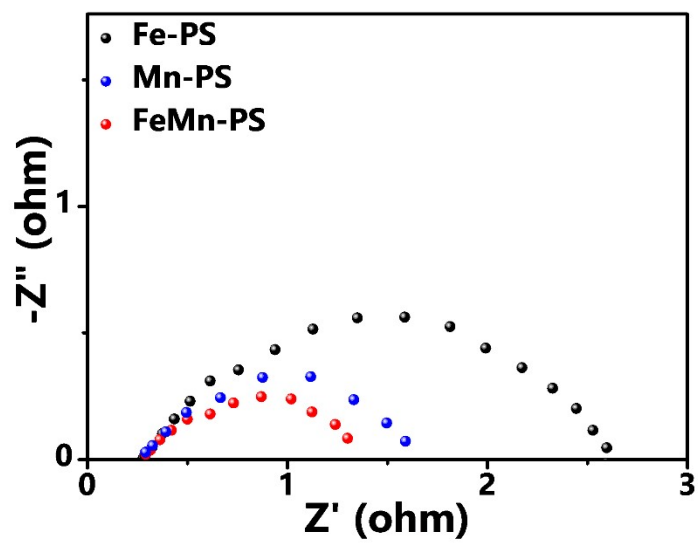
Fig. S11. Nyquist plots of Fe-PS, Mn-PS and FeMn-PS for UOR test at 1.5 V vs. RHE over a frequency range of 10^5 to 10^{-2} Hz.

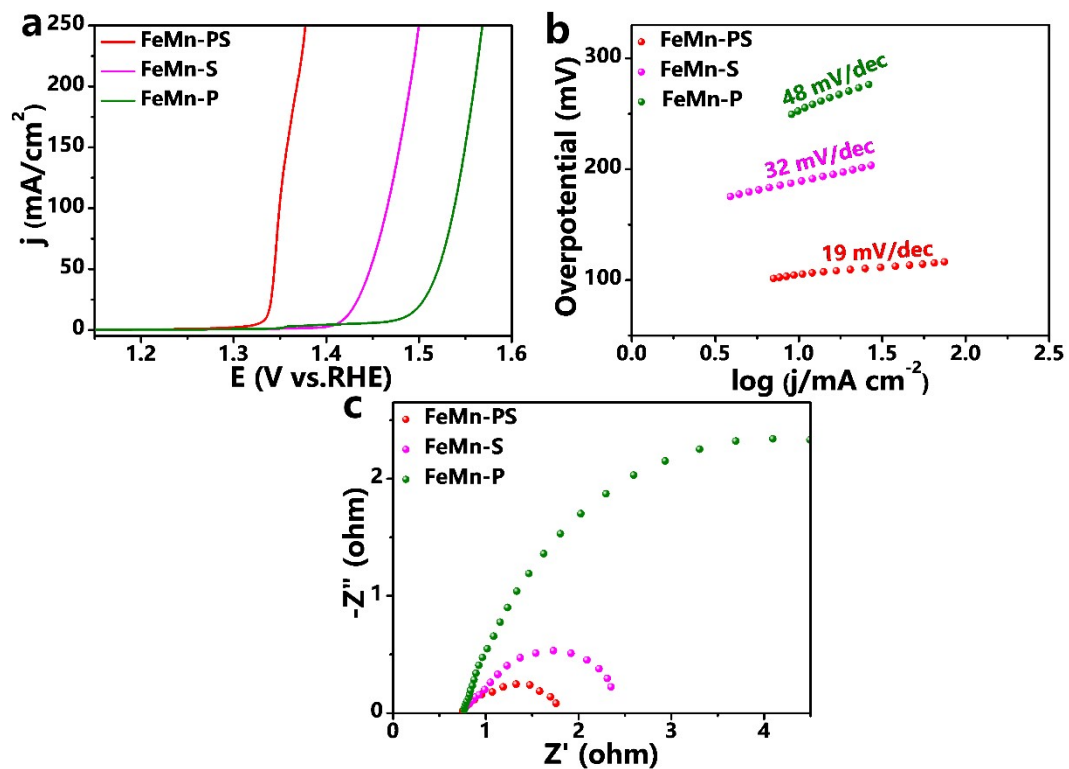**Fig. S12**. UOR performance. (a) Polarization curves of FeMn-PS, FeMn-S and FeMn-P in Ar-saturated 0.33 M urea electrolyte. (b) Tafel plots of FeMn-PS, FeMn-S and FeMn-P. (c) Nyquist plots of FeMn-PS, FeMn-S and FeMn-P.
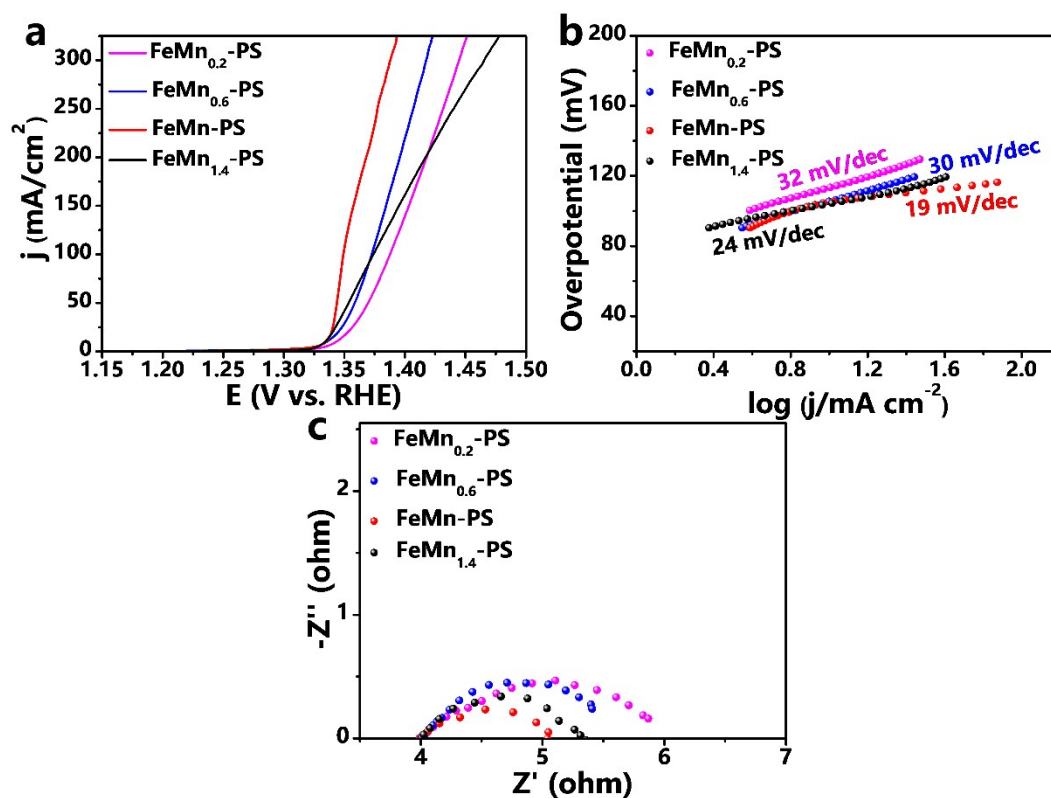
Fig. S13. (a) UOR polarization curves, (b) corresponding Tafel plots and (c) Nyquist plots of pristine FeMn$_{0.2}$-PS, FeMn$_{0.6}$-PS, FeMn-PS, FeMn$_{1.4}$-PS in 1 M KOH with 0.33 M urea.
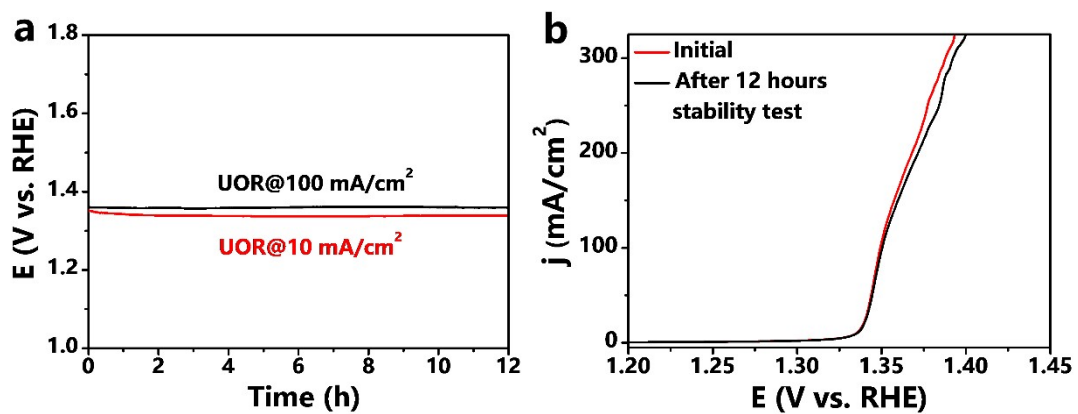
Fig. S14. (a) Chronopotentiometric curves of FeMn-PS in 1 M KOH electrolyte with 0.33 M urea. (b) LSV curves of the FeMn-PS initial and after 12 hours stability test in 1 M KOH with 0.33 M urea.

Fig. S15. SEM images of FeMn-PS after chronopotentiometry test of (a) OER and (b) UOR. (c) Raman spectrum of FeMn-PS after chronopotentiometry test of OER and UOR.

Fig. S16. XPS spectra of FeMn-PS catalysts: (a) Fe 2p, (b) Mn 2p, (c) O 1s, (d) P 2p and (e) S 2p after OER and UOR test.

Table S1. Comparison of the OER and UOR performances with other reported non-noble electrocatalysts .

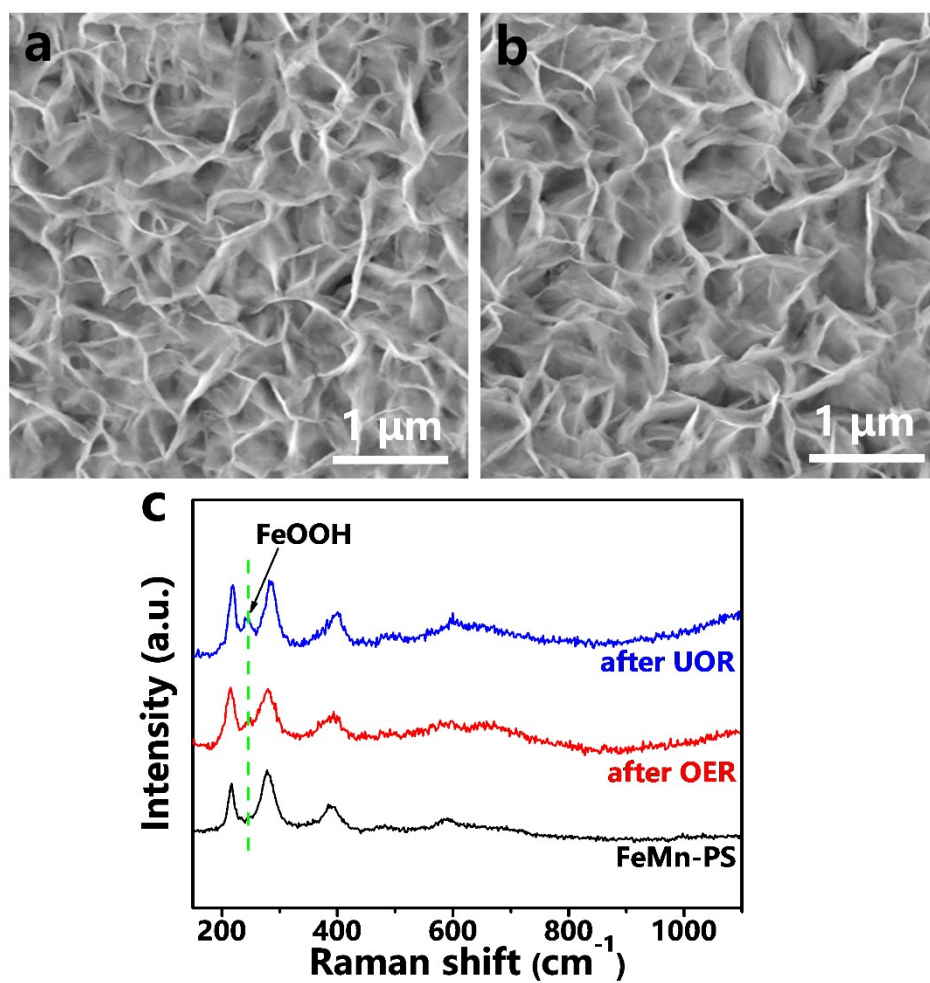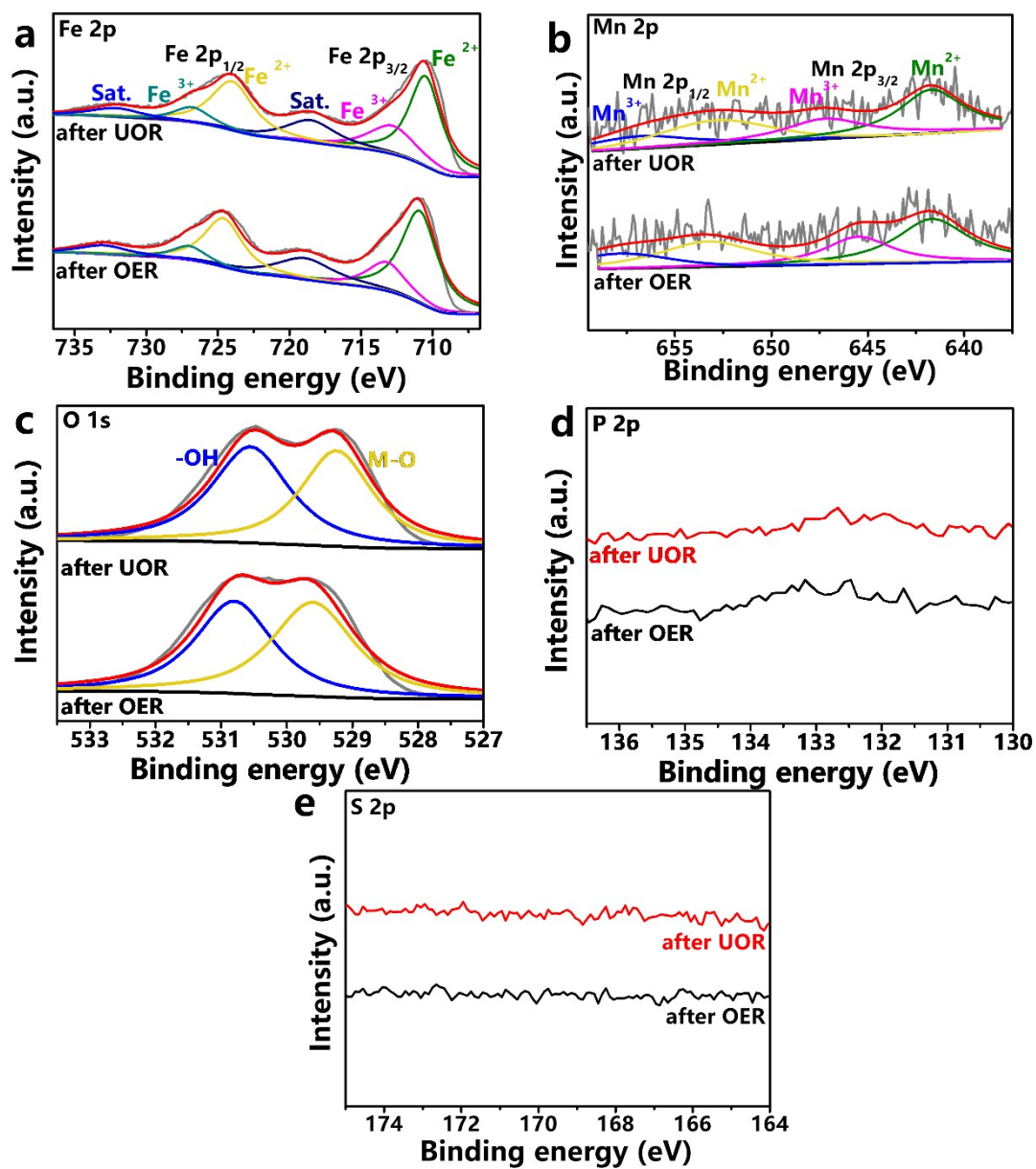| Catalysts	support	OER		UOR		Ref.
		η_{100}[a]	Tafel slope (mV dec^{-1})	E_{10}[b]	Tafel slope (mV dec^{-1})	
FeMn-PS	NF	237	59	1.33	19	This work
pa-NiFe LDH NS/NIF	NF	326	38	1.34	33	1
Fe$_{11.1\%}$–Ni$_3$S$_2$	NF	252	62	1.52	-	2
N, S-doped carbon-MnFe$_2$O$_4$	Glass carbon	410	-	1.37	44	3
Fe-Ni$_3$S$_2$@FeNi$_3$-8	FeNi$_3$ foam	280	83	1.40	29	4
FeOOH	NF	330	97	1.37	26	5
Se-MnS/NiS	NF	317	50	-	-	6
Mn$_3$(PO$_4$)$_2$·3H$_2$O	FTO	> 680	120	-	-	7
(Fe$_{1-x}$, Mn$_x$)OOH	FTO	390	71	-	-	8
Mn$_3$O$_4$/Fe$_2$O$_3$	NF	615	46	-	-	9
S-MnO$_2$	NF	-	-	1.34	75	10
Ni$_{0.9}$Fe$_{0.1}$O$_x$ microspheres	CFP	-	-	1.37	26	11
Ni$_2$P/Fe$_2$P	NF	-	-	1.36	79	12
NiMn-decorated activated carbon	-	-	-	1.47	-	13

a Overpotential corresponding to current density in brackets

b Voltage corresponding to current density in brackets

References

1. J. Xie, H. Qu, F. Lei, X. Peng, W. Liu, L. Gao, P. Hao, G. Cui and B. Tang, *Journal of Materials Chemistry A*, 2018, **6**, 16121-16129.

2. W. Zhu, Z. Yue, W. Zhang, N. Hu, Z. Luo, M. Ren, Z. Xu, Z. Wei, Y. Suo and J. Wang, *Journal of Materials Chemistry A*, 2018, **6**, 4346-4353.

3. P. Balasubramanian, A. Jansirani, S.-B. He, H.-H. Deng, H.-P. Peng, X.-H. Xia and W. Chen, *Journal of Power Sources*, 2021, **494**, 229757-229764.

4. W. Zhang, Q. Jia, H. Liang, L. Cui, D. Wei and J. Liu, *Chemical Engineering Journal*, 2020, **396**, 125315-125326.

5. J.-J. Zhang, W.-W. Bao, M.-Y. Li, C.-M. Yang and N.-N. Zhang, *Chemical Communications*, 2020, **56**, 14713-14716.

6. J. Zhu, M. Sun, S. Liu, X. Liu, K. Hu and L. Wang, *Journal of Materials Chemistry A*, 2019, **7**, 26975-26983.

7. K. Jin, J. Park, J. Lee, K. D. Yang, G. K. Pradhan, U. Sim, D. Jeong, H. L. Jang, S. Park, D. Kim, N.-E. Sung, S. H. Kim, S. Han and K. T. Nam, *Journal of the American Chemical Society*, 2014, **136**, 7435-7443.

8. M. P. Suryawanshi, U. V. Ghorpade, S. W. Shin, U. P. Suryawanshi, H. J. Shim, S. H. Kang and J. H. Kim, *Small*, 2018, **14**, 1801226.

9. J. Luo, W. H. Guo, Q. Zhang, X. H. Wang, L. Shen, H. C. Fu, L. L.

Wu, X. H. Chen, H. Q. Luo and N. B. Li, *Nanoscale*, 2020, **12**, 19992-20001.

10. S. Chen, J. Duan, A. Vasileff and S. Z. Qiao, *Angewandte Chemie International Edition*, 2016, **55**, 3804-3808.

11. F. Wu, G. Ou, J. Yang, H. Li, Y. Gao, F. Chen, Y. Wang and Y. Shi, *Chemical Communications*, 2019, **55**, 6555-6558.

12. L. Yan, Y. Sun, E. Hu, J. Ning, Y. Zhong, Z. Zhang and Y. Hu, *Journal of Colloid and Interface Science*, 2019, **541**, 279-286.

13. N. A. M. Barakat, M. Alajami, Y. Al Haj, M. Obaid and S. Al-Meer, *Catalysis Communications*, 2017, **97**, 32-36.